Journal of Hydrology 519 (2014) 340–352

Contents lists available at ScienceDirect

Journal of Hydrology

journal homepage: www.elsevier.com/locate/jhydrol

Tracking water pathways in steep hillslopes by $\delta^{18}O$ depth profiles of soil water

Matthias H. Mueller [a,*], Abdallah Alaoui [b], Christoph Kuells [c,1], Hannes Leistert [c], Katrin Meusburger [a], Christine Stumpp [d], Markus Weiler [c], Christine Alewell [a]

[a] Environmental Geosciences, University of Basel, Bernoullistrasse 30, 4056 Basel, Switzerland
[b] Centre for Development and Environment (CDE), University of Bern, Hallerstrasse 10, 3012 Bern, Switzerland
[c] Chair of Hydrology, University of Freiburg, Fahnenbergplatz, 79098 Freiburg, Germany
[d] Helmholtz Zentrum München, Institute of Groundwater Ecology, Ingolstädter Landstr. 1, 85764 Neuherberg, Germany

ARTICLE INFO

Article history:
Received 5 October 2013
Received in revised form 11 July 2014
Accepted 15 July 2014
Available online 24 July 2014
This manuscript was handled by Peter K. Kitanidis, Editor-in-Chief, with the assistance of J. Simunek, Associate Editor

Keywords:
Stable isotopes
Soil water
Steep hillslopes
Modeling
Water pathways
Snowmelt

SUMMARY

Assessing temporal variations in soil water flow is important, especially at the hillslope scale, to identify mechanisms of runoff and flood generation and pathways for nutrients and pollutants in soils. While surface processes are well considered and parameterized, the assessment of subsurface processes at the hillslope scale is still challenging since measurement of hydrological pathways is connected to high efforts in time, money and personnel work. The latter might not even be possible in alpine environments with harsh winter processes. Soil water stable isotope profiles may offer a time-integrating fingerprint of subsurface water pathways. In this study, we investigated the suitability of soil water stable isotope ($\delta^{18}O$) depth profiles to identify water flow paths along two transects of steep subalpine hillslopes in the Swiss Alps. We applied a one-dimensional advection–dispersion model using $\delta^{18}O$ values of precipitation (ranging from −24.7 to −2.9‰) as input data to simulate the $\delta^{18}O$ profiles of soil water. The variability of $\delta^{18}O$ values with depth within each soil profile and a comparison of the simulated and measured $\delta^{18}O$ profiles were used to infer information about subsurface hydrological pathways. The temporal pattern of $\delta^{18}O$ in precipitation was found in several profiles, ranging from −14.5 to −4.0‰. This suggests that vertical percolation plays an important role even at slope angles of up to 46°. Lateral subsurface flow and/or mixing of soil water at lower slope angles might occur in deeper soil layers and at sites near a small stream. The difference between several observed and simulated $\delta^{18}O$ profiles revealed spatially highly variable infiltration patterns during the snowmelt periods: The $\delta^{18}O$ value of snow (−17.7 ± 1.9‰) was absent in several measured $\delta^{18}O$ profiles but present in the respective simulated $\delta^{18}O$ profiles. This indicated overland flow and/or preferential flow through the soil profile during the melt period. The applied methods proved to be a fast and promising tool to obtain time-integrated information on soil water flow paths at the hillslope scale in steep subalpine slopes.

1. Introduction

Knowledge about soil water flow paths is important to assess mechanisms of runoff generation (Stewart and McDonnell, 1991), which include for example overland and subsurface flow (Dunne, 1978). These processes subsequently have important implications for the generation of floods (Beven, 1986), recharge of groundwater (Barnes and Allison, 1988), soil erosion dynamics (e.g. Konz et al., 2010; Lindenmaier et al., 2005; Uchida et al., 2001) and transport of nutrients and pollutants (Schmocker-Fackel, 2004; Weiler and McDonnell, 2006). These processes are of special interest in headwater catchments in mountainous regions, because of their great hydrological importance for the adjacent lowlands (Viviroli et al., 2011; Weingartner et al., 2007).

Hydrological processes at the hillslope scale are influenced by a complex interplay of different factors, including input characteristics, vegetation, geological, morphological and pedological characteristics, all acting on different spatial and temporal scales

* Corresponding author. Present address: Applied and Environmental Geology, University of Basel, Bernoullistrasse 32, 4056 Basel, Switzerland. Tel.: +41 61 267 35 95.

E-mail addresses: matthiash.mueller@unibas.ch (M.H. Mueller), abdallah.alaoui@cde.unibe.ch (A. Alaoui), christoph.kuells@hydrology.uni-freiburg.de (C. Kuells), hannes.leistert@hydrology.uni-freiburg.de (H. Leistert), Katrin.Meusburger@unibas.ch (K. Meusburger), christine.stumpp@helmholtz-muenchen.de (C. Stumpp), markus.weiler@hydrology.uni-freiburg.de (M. Weiler), Christine.Alewell@unibas.ch (C. Alewell).

[1] Present address: University of Applied Sciences, Mönkhofer Weg 239, 23562 Lübeck, Germany.

http://dx.doi.org/10.1016/j.jhydrol.2014.07.031
0022-1694/

(Bachmair and Weiler, 2011). Among the topographic controls, slope angle has been identified as a crucial factor influencing hillslope hydrology, i.e. water flows paths (e.g. Hopp and McDonnell, 2009; Lv et al., 2013; Penna et al., 2009). Further, Sayama et al. (2011) found that storage of water was increased with increasing catchment slope. This was due to a greater extent of hydrological active (permeable) bedrock, which is available for water storage in steeper catchments. This underpins the hydrological importance of headwater catchments and the necessity to obtain information on (subsurface) water pathways in these areas. Moreover, Vereecken et al. (2008), UNESCO-IHE (2011) highlight the importance of knowledge about spatial distribution of hydrological processes and characteristics in the subsurface at different spatial scales.

A great variety of techniques has been applied to study soil hydrological processes. Soil water content can be monitored e.g. by time-domain reflectometry (TDR), electrical resistivity measurements, heat pulse sensors or capacitive sensors (for a review see Vereecken et al., 2008). However, to obtain information on soil water content dynamics at the hillslope scale using these techniques, a high number of sensors has to be deployed during a relatively long time period measuring with high temporal resolution (see review of Dobriyal et al., 2012; Zehe et al., 2010). In addition, the use of hydrometric equipment may be limited in stony soils (Coppola et al., 2013) or due to harsh winter conditions, which often occur in steep hillslopes in alpine headwater catchments. Spatially distributed information on areas where water flow potentially concentrates, can be derived from the topographic wetness index TWI (Beven and Kirkby, 1979), calculated from a digital elevation model. However, Penna et al. (2009) found that flow-related topographic variables (e.g. slope, contributing area and wetness index) could only explain up to 42% of the spatial variation of soil moisture in steep mountainous terrain during two summer seasons. In addition to surface topography, the subsurface topography also plays a crucial role for water flow paths (Freer et al., 2002). Ground penetrating radar (GPR) or electrical resistivity tomography (ERT) can indirectly provide information about possible flow paths in the subsurface, soil water contents, hydraulic properties and soil water dynamics (Jadoon et al., 2012; Lunt et al., 2005; Steelman and Endres, 2012). However, heterogeneities in soils can limit accurate assessment of subsurface characteristics by GPR (Jadoon et al., 2012). All these techniques require a high effort in time, work and economic resources if a monitoring of water fluxes in various compartments over several seasons is investigated (e.g. long-term high-frequency measurements).

Alternatively, soil water stable isotopes can be a valuable tool to track movement of soil water and to gain integrative information about subsurface flow processes like mixing, preferential flow and hydrodynamic dispersion (Asano et al., 2002; Barnes and Allison, 1988; Dusek et al., 2012; Klaus et al., 2013; McDonnell et al., 1991; Stewart and McDonnell, 1991; Stumpp and Maloszewski, 2010; Stumpp et al., 2009). The seasonally varying stable isotope signals of precipitation and the subsequent potential attenuation or propagation of distinct peaks in the soil water can be used to determine recharge rates (Adomako et al., 2010; McConville et al., 2001; Saxena and Dressie, 1983), soil water movement (Gehrels et al., 1998) and to calculate soil water transit times (Stewart and McDonnell, 1991; Stumpp et al., 2012). As such, pore water stable isotope signals have the potential to give a fingerprint integrating over time (one season to several years) and a certain space.

Soil water for stable isotope analysis can be extracted by suction lysimeters (Stewart and McDonnell, 1991), centrifugation of soil samples (Gehrels et al., 1998) or distillation techniques (Ingraham and Shadel, 1992), which are time-consuming and prone to isotopic fractionation (Wassenaar et al., 2008). Wassenaar et al. (2008) developed a fast and effective method for soil water stable isotope analysis, which is based on H_2O_{liquid}–H_2O_{vapor} equilibration laser spectroscopy. Garvelmann et al. (2012) applied this approach and used a combination of soil water stable isotope profiles along two relatively smooth hillslope transects and digital terrain analysis to investigate subsurface hydrological processes. With these methods they were able to deduce the relative importance of dominant subsurface flow paths (vertical percolation and lateral subsurface flow) at the hillslope scale. Their approach offers a way to generate a time-integrated overview of soil water flow paths in the subsurface without the need of extensive hydrometric equipment. However, a more physically based description of soil water flow and transport processes to support their conceptual model was not realized in their study. The Richards equation for variably-saturated flow combined with advection–dispersion equations can be used to quantitatively describe water flow and solute transport in soils (e.g. van Genuchten and Simunek, 2004). More complex models to account for non-equilibrium and preferential flow include for example dual-porosity and dual-permeability approaches (for reviews see Beven and Germann, 2013; Simunek et al., 2003). Stable isotopes of soil water in combination with modeling tools were successfully used to describe soil hydrological processes at the plot scale (e.g. Shurbaji and Phillips, 1995; Stumpp et al., 2012) and the hillslope scale (e.g. Dusek et al., 2012). Studies on the plot scale using lysimeters give detailed information on transport parameters on the one hand (e.g. Stumpp et al., 2012). Studies on hillslope hydrographs provide integrated information at the hillslope scale (e.g. Dusek et al., 2012), missing the spatial variability of e.g. transport parameters on the other hand. A method linking this gap could provide important additional information that can be included in detailed spatial hydrological models at the hillslope scale. The aims of the presented study were therefore: (i) to use depth profiles of soil pore water stable isotopes as an indicator of water flow paths and its heterogeneity at the hillslope scale, (ii) to combine measurements of stable water isotopes of soil profiles with a numerical model of the Richards equation coupled with the advection–dispersion equation including fractionation processes to identify water pathways and transport processes in the shallow subsurface and (iii) to apply this method in steep hillslopes in a remote alpine headwater catchment, where installation of more conventional equipment to investigate water flow and solute transport would not only be extremely time consuming but also very difficult (e.g. due to harsh winter conditions, which can impede continuous measurements or due to high stone contents, which might hamper proper installation of TDR probes). The method was tested with 28 depth profiles of soil water $\delta^{18}O$ values at a transect of a north- and a south-facing subalpine hillslope in the Swiss Alps. The suggested method is designed as a diagnostic tool to obtain a time-integrated overview of hillslope hydrology, without the necessity to collect long time series data of hillslope hydrology.

2. Material and methods

2.1. Study site

Soil samples for analysis of soil water stable isotopes were taken on two opposing hillslopes in the Urseren Valley in the Central Alps, Switzerland (Fig. 1). The U-shaped valley is characterized by a rugged terrain. Its main axis is parallel to a geological fault line which separates the granites of the Aar massif and the gneisses of the so-called Altkristallin from the paragneisses and granites of the Gotthard massif (Labhart, 1977). The two massifs are separated by softer Permocarbonic and Mesozoic sediments, the so-called Urseren Zone (Labhart, 1977). These vertically dipping layers consist of Permocarbonic sandy-clay sediments and Mesozoic sandstones, rauhwackes, dolomites, dark clay–marl, marl, clays and limestones.

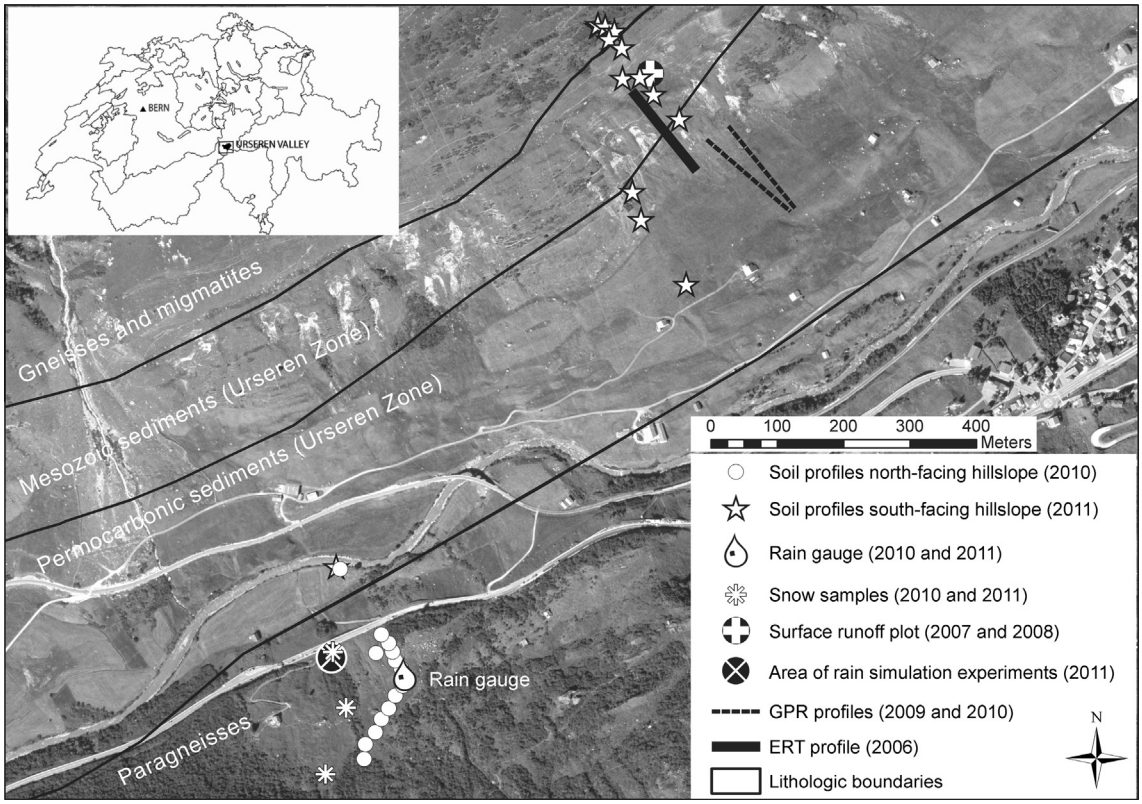

Fig. 1. Location of the Urseren Valley and the investigated hillslopes. Locations of selected ground penetrating radar profiles (GPR) and the electrical resistivity tomography profile (ERT) are indicated; data from Carpentier et al. (2012). Air photograph reproduced by permission of Swisstopo (BA13058).

Quaternary alluvium can be found at the lower parts of the valley slopes. The south-east-facing hillslope (named south-facing in the following) includes the gneisses of the Altkristallin and the sediments of the Urseren Zone in the lower part. The north-west-facing hillslope (named north-facing in the following) is underlain by the paragneissic rocks of the Gotthard massif. In the summers 2006, 2009 and 2010 Carpentier et al. (2012) collected data with ground penetrating radar (GPR), electrical resistivity tomography (ERT) and direct observations in soil trenches at a section of the south-facing hillslope (Fig. 1). They detected a xenolithic schist layer starting mostly at 1 m depth followed by a clay layer at about 2 m depth. They also detected some vertical structures which were interpreted as faults/fractures in the bedrock or vertically dipping layers due to interbedding in the schistose rocks. These structures can enhance infiltration of water into deeper zones of the bedrock, which starts at 2.5 m depth in the upper part and 10 m depth in the lower part of the investigated hillslope section. Slope angles of the investigated sites range from 5° to 29° and from 3° to 46° at the north and the south-facing hillslope, respectively.

The dominant soil types in the Urseren Valley according to the world reference base (IUSS Working Group WRB, 2006) are Podsols and Cambisols (Meusburger and Alewell, 2008). Leptosols developed at higher elevations and steeper slopes. Clayey gleyic Cambisols, Histosols, Fluvisols and Gleysols are commonly associated with the valley bottom and downslope areas. Soils on the investigated north-facing hillslope can be described as Podsols partially with gleyic or slight histic properties. Soils on the south-facing hillslope are mainly Cambisols. The latter can partially be affected by a clay layer in deeper zones of about 2 m depth, possibly impeding downward water flow (Carpentier et al., 2012). Generally, soils in the Urseren Valley are high in silt and sand content with relatively low content of clay (Gysel, 2010).

The hydrometeorological conditions in the Urseren Valley are characterized by an alpine climate with precipitation rather evenly distributed over the year. Mean annual air temperature at the MeteoSwiss climate station in Andermatt (1442 m a.s.l., years 1980–2012) is 4.1 ± 0.7 °C and mean annual precipitation is 1457 ± 290 mm, with ~30% falling as snow (MeteoSwiss, 2013). The period of snow cover lasts usually from November to April.

Vegetation was strongly influenced by pasturing for centuries (Kägi, 1973). An invasion of shrubs after reduced grazing was identified for both, the north and south-facing slopes along the valley. Particularly on the north-facing slopes shrubs are predominant (Kägi, 1973; Küttel, 1990; Wettstein, 1999). The south-facing slopes are dominated by dwarf-shrub communities (Kägi, 1973; Küttel, 1990) and diverse herbs and grass species. Both investigated hillslopes of this study are mainly covered by grassland.

2.2. Sampling and analysis

2.2.1. $\delta^{18}O$ of precipitation

We monitored $\delta^{18}O$ values in precipitation (volume integrated) at the north-facing hillslope and used these $\delta^{18}O$ data as input data to simulate the $\delta^{18}O$ profiles of soil water (described in Section 2.2.3). Precipitation was sampled biweekly with a 0.02 m^2 seasonal rain gauge and a buried and covered 5 L bottle to protect the water from evaporation. Snow was collected as bulk samples on a monthly basis during the winter with a plastic tube of 2 m length and a diameter of 0.035 m at the lowest point of the north-facing hillslope. In March 2010 and 2011, we additionally sampled snow spatially distributed over several kilometers along the valley slopes from 1500 to 2700 m a.s.l. to account for spatial heterogeneity of stable isotopes in snow. The south-facing hillslope was not sampled for snow due to high avalanche risk in the lower parts of the south-facing slopes. However, snow samples from May 2011 of an avalanche-safe area at a south-facing slope at 2400 m a.s.l. (about 8 km west from the investigated hillslope) were available. These samples were used to estimate the $\delta^{18}O$ values in snow cover

at the south-facing hillslope. $\delta^{18}O$ values in precipitation (snow was melted) were measured with a Thermo Finnigan GasBench II connected to a Thermo Finnigan DELTAplus XP continuous flow mass spectrometer (CF-IRMS, DELTAplus XP, Thermo, Bremen, Germany) and a liquid water isotope analyzer (Los Gatos Research, Inc. (LGR), Mountain View, USA). Results are reported as $\delta^{18}O$ in ‰ versus the V-SMOW (Vienna Standard Mean Ocean Water) standard. Precisions were 0.05‰ with the IRMS and 0.1‰ with the LGR instrument. The precisions are calculated based on long term performance of the instruments, using multiple injections of the applied standards V-SMOW, SLAP and GISP. The measured samples were then calibrated to these standards.

2.2.2. $\delta^{18}O$ of soil water

In August 2010, we took soil samples from 15 soil profiles with a 0.9 m long soil corer of 0.055 m diameter. Samples were taken on two consecutive days along a transect at a north-facing hillslope (Fig. 1). About 20 mm of rainfall occurred on the second sampling day (profiles 22–27a; more details will be discussed below). In June 2011, 13 profiles were taken along a south-facing hillslope transect (Fig. 1). The samples at the foot of the south-facing hillslope were slightly relocated in relation to the samples from the upper part, which was due to agricultural land use in the lower area. Soil cores were transported to the laboratory in sealed plastic tubes to prevent evaporation. They were stored 3 days at 4 °C until analysis, due to practical constraints. For stable isotope analysis of soil water ($\delta^{18}O$), we followed the procedure described by Garvelmann et al. (2012), which is based on the H_2O_{liquid}–H_2O_{vapor} equilibration and laser spectroscopy method used by Wassenaar et al. (2008). We took subsamples of the soil cores at 0.05–0.1 m intervals and placed the fresh subsamples into two nested 1 L Ziplock plastic bags. In 2011, the Ziplock were replaced by laminated polyester bags (Weber Packaging, Germany), which were heat-sealed. The polyester bags we used in 2011 are easier to handle and less susceptible to gas losses. Prior to analysis each bag was filled with dried air and left for 15 h in the laboratory to reach equilibrium of stable isotopes between soil water and water vapor in the bags. Stable isotope analysis of the headspace water vapor ($\delta^{18}O$) of the soil samples was performed via Wavelength-Scanned Cavity Ring Down Spectroscopy (WS-CRDS, Picarro, USA). Precision for this analysis was 0.16‰ versus V-SMOW.

In 2010, the calibration of raw soil water $\delta^{18}O$ values from the north-facing hillslope was performed by using the fractionation factor α between H_2O_{liquid} and H_2O_{vapor}, the respective equilibration coefficients from Majoube (1971), and the measured equilibration temperature in the laboratory. The coefficients from Majoube (1971) will be given below, together with the description of the soil water stable isotope model. With these values we calculated the $\delta^{18}O$ values of the soil pore water from the respective signals of the headspace water vapor.

In 2011, the calibration procedure was modified. For the standards, we applied water with a known $\delta^{18}O$ value to dried soil samples from the site ($n = 23$) and treated them in the same way as the actual samples. This allowed direct calculation of $\delta^{18}O$ values of soil water by relating the measured $\delta^{18}O$ value of the water vapor of the spiked calibration samples to the real, known $\delta^{18}O$ value of the applied liquid water of these spiked calibration samples. These spiked samples were used to re-check the calibration method from 2010 using the fractionation factors. The $\delta^{18}O$ value of the applied liquid water was reproduced with a mean standard error of 0.5‰ versus V-SMOW, which is considered as the accuracy of our method. This cross-check of the calibration methods underpins the validity of the calibration method from 2010 using the fractionation factors. Additionally, repeated measurements on 15 selected samples within a few hours showed that the mean difference between the first and the second measurement of the same sample was 0.3‰ versus V-SMOW.

Variability of the measured soil water $\delta^{18}O$ profiles was analyzed by comparing the coefficients of variation (CV) of the profiles. The CV was calculated according to the equation suggested by Fry (2003) which is used for natural abundance samples applying the stable isotope ratios R ($^{18}O/^{16}O$) of the samples:

$$CV = \left(\frac{R_{stdev}}{R_{mean}}\right) \cdot 1000‰, \tag{1}$$

where R_{stdev} is the standard deviation and R_{mean} is the mean of measured stable isotope ratios respectively.

2.2.3. Modeling of soil water $\delta^{18}O$ profiles

The soil water flow was modeled based on a numerical solution of the nonlinear Richards equation (Richards, 1931) for unsaturated water flow in the vadose zone:

$$\frac{\partial\theta(t)}{\partial t} = \frac{\partial}{\partial z}\left(k(\psi(\theta(t))) * \left(\frac{\partial\psi(\theta(t))}{\partial z} - 1\right)\right) - ET_a, \tag{2}$$

where θ is the water content, q is the water flux, $\psi(\theta)$ is the matrix potential as a function of water content, $k(\psi(\theta))$ is the unsaturated hydraulic conductivity as a function of the matrix potential and ET_a is the actual evapotranspiration.

Unsaturated hydraulic conductivity $k(\psi(\theta))$ and matrix potential $\psi(\theta)$ as functions of the water content θ were calculated based on the Mualem–van Genuchten approach (Mualem, 1976; Van Genuchten, 1980). The Mualem–van Genuchten parameters, which include saturated and residual water contents and empirical parameters, were chosen based on the textural classes according to Sponagel et al. (2005), Renger et al. (2009).

ET_a was calculated based on potential evapotranspiration (ET_p) and water availability according to the approach implemented in WASIM-ETH (Schulla and Jasper, 2007) and in TOPMODEL (Menzel, 1997). Thus, potential evapotranspiration (ET_p) was calculated using the Hargreaves equation (Hargreaves and Samani, 1982). Evapotranspiration was split into evaporation with isotope fractionation and transpiration without fractionation. The latter may still influence the stable isotope profile of soil water indirectly, as a result of partial removal of soil water and a subsequently modified soil water flow. Transpiration was set to 70% of evapotranspiration during the growing season, and 10% of evapotranspiration during the dormant season, which is based on estimates for alpine grasslands of Körner et al. (1989). Transpiration was implemented with a linear root water uptake function with depth. The amount of precipitation or snowmelt that exceeds the infiltration capacity is allocated to a runoff component. As the model is one dimensional this runoff component is not redistributed downhill.

The one-dimensional differential advection–dispersion equation was used to calculate isotope transport:

$$\frac{\partial\theta C}{\partial t} = \frac{\partial}{\partial z}\left(\theta D\frac{\partial C}{\partial z}\right) - \frac{\partial(qC)}{\partial z} - (EC_f + TC), \tag{3}$$

where C corresponds to the ^{18}O content of soil water (in atom%) and C_f is the fractionated evaporation concentration (atom%, description see below), E represents the soil evaporation, T the plant transpiration, q the water flux and D the dispersion coefficient. The latter was calculated as:

$$D = \frac{\lambda \cdot q}{\theta}, \tag{4}$$

with λ = dispersivity.

Conversion of the isotope values, given as delta values ($\delta^{18}O$), into atom% ratios and back calculation after the simulation runs, was done using the isotope ratios of the standard V-SMOW, using the following equation:

$$C(\text{atom}\%) = \frac{\left(\frac{\delta^{18}O}{1000}+1\right)\cdot R_{std}}{1+\left(\frac{\delta^{18}O}{1000}+1\right)\cdot R_{std}}\cdot 100\%, \quad (5)$$

with R_{std} being the isotope ratio $^{18}O/^{16}O$ of the standard.

Equilibrium and kinetic isotope fractionation were considered and solved for. Therefore, the equilibrium fractionation factor $\alpha_{18O\_liquid\text{-}vapor}$ was calculated according to the coefficients $a_{18O} = 1.137$, $b_{18O} = -0.4156$ and $c_{18O} = -2.0667$, determined by Majoube (1971) as a function of ambient temperature T:

$$\alpha_{18O\_liquid-vapor} = \exp\left[\left(\frac{a_{18O}\cdot 10^6}{T^2}+\frac{b_{18O}\cdot 10^3}{T}+c_{18O}\right)\cdot\frac{1}{10^3}\right]. \quad (6)$$

Additional kinetic fractionation by non-equilibrium fractionation for ^{18}O was calculated based on the approximation of Gonfiantini (1986) as a function of humidity h (available from the MeteoSwiss station in Andermatt) and then converted to a kinetic fractionation factor α_{k_18O} using the enrichment factor ε_{k_18O} (see Eqs. (8) and (9)). Kinetic fractionation is assumed to occur only in the upper 0.1 m of the soil.

$$\varepsilon_{k\_18O} = 14.2\cdot(1-h), \quad (7)$$

$$\alpha_{k\_18O} = \alpha_{18O\_liquid-vapor} + \left(\frac{\varepsilon_{k\_18O}}{1000}\right), \quad (8)$$

The fractionated evaporation concentration C_f was then calculated using the isotope ratios R ($^{18}O/^{16}O$) of water vapor and liquid water and the fractionation factor α_{k_18O} as:

$$R_{vapor} = \frac{R_{liquid}}{\alpha_{k\_18O}}. \quad (9)$$

The soil profile was subdivided into 12 cells of 0.1 m depth each and the model was run with a daily time step. Daily $\delta^{18}O$ values of precipitation were calculated from air temperature data and their correlation to the biweekly measured stable isotope signature of precipitation from the period March 2010 to March 2012 ($\delta^{18}O = 0.73\cdot T$ (°C)–16.89, $r^2 = 0.84$, $p < 0.0001$, $n = 145$). For the regression analysis, the precipitation-weighted arithmetic mean of air temperature of the respective biweekly interval was calculated by using measured daily air temperatures and daily precipitation volumes. This was done in order to consider only days with precipitation in the regression analysis. For the model input of the soil water stable isotopes in this study, the $\delta^{18}O$ values were weighted with precipitation volume via Eqs. (2) and (3). Infiltration of precipitation into the soil was set to zero during the winter seasons, when snow accumulated. The daily snowmelt volume in spring was estimated according to the degree-day-method (Linsley, 1943) using daily air temperatures. We slightly modified the degree-day-method by scaling the sum of calculated total snowmelt volume to the total measured snow water equivalent at the MeteoSwiss station in Andermatt. We obtained daily snowmelt rates of 10 ± 13 mm day^{-1} (mean ± standard deviation) for the south-facing hillslope (year 2011) and 13 ± 13 mm day^{-1} for the north-facing hillslope (year 2010). Fractionation effects during the snowmelt period were introduced by assuming that the first melt water was depleted by 2‰ compared to the measured $\delta^{18}O$ values of the bulk snow samples for the north- and the south-facing hillslope. These estimates are based on comparison of measured bulk snow samples at the beginning and the end of the snow accumulation period and following the estimates of Taylor et al. (2001), who investigated the stable isotope fractionation during snowmelt.

Two different input parameter sets were considered for the simulation runs to test the influence of the snowmelt component on the $\delta^{18}O$ profiles. The first input set ("sim1") refers to the $\delta^{18}O$ input as described above, including the snowmelt component. The second input set "sim2" refers to a data set from which we excluded the entire snowmelt component, which might not have entered (e.g. overland flow) or bypassed the soil matrix. We consider the two data sets "sim1" and "sim2" as extreme scenarios.

The model efficiency was evaluated using the Nash–Sutcliffe efficiency coefficient (NSE) (Nash and Sutcliffe, 1970):

$$NSE = 1 - \frac{\sum_{z=1}^{n}\left(\delta^{18}O_{z,obs} - \delta^{18}O_{z,sim}\right)^2}{\sum_{z=1}^{n}\left(\delta^{18}O_{z,obs} - \delta^{18}O_{mean,obs}\right)^2}, \quad (10)$$

where $\delta^{18}O_{z,\ sim}$ is the simulated $\delta^{18}O$ value at depth z, $\delta^{18}O_{z,\ obs}$ is the measured $\delta^{18}O$ value at depth z, $\delta^{18}O_{mean,\ obs}$ is the mean of the observed values, and n is the number of measured and simulated $\delta^{18}O$ values. Additionally, measured and simulated $\delta^{18}O$ profiles were compared using the root mean squared error (RMSE):

$$RMSE = \sqrt{\frac{1}{n}\sum_{z=1}^{n}\left(\delta^{18}O_{z,sim} - \delta^{18}O_{z,obs}\right)^2}. \quad (11)$$

A good agreement between measured and simulated $\delta^{18}O$ profiles (NSE close to 1 and low RMSE) consequently indicates a good model performance and that vertical soil water flow can be simulated well within a soil profile. Poor model efficiency suggests that either other flow processes take place which are not captured by the applied one dimensional model or that the chosen parameters for vertical flow are not representative.

2.2.4. Physical and hydrological soil properties

Homogenized, dried and sieved (2 mm) soil samples from 0 to 0.55 m depth from locations of the north- and south-facing slopes across the Urseren Valley were used for grain size analyses. We used sieves for grain sizes between 32 and 2000 μm and a Sedigraph 5100 (Micromeritics) for grain sizes between 1 and 32 μm. Samples were treated with H_2O_2 to oxidize organic carbon and sodium hexametaphosphate to break soil aggregates prior to analysis (König, 2009). Soil texture classes of the sampled depth profiles of the two hillslopes were estimated in the laboratory by a quick finger method described by Sponagel et al. (2005). Skeleton content, i.e. particles >2 mm, was determined gravimetrically. Saturated hydraulic conductivity (K_{sat}) of undisturbed soil samples from grassland sites on the north-facing hillslope from 0 to 0.15 m and 0.2 to 0.35 m depth was determined in the laboratory with a constant head permeameter (Klute and Dirksen, 1986). 12 samples were measured for each depth interval.

Additional soil hydrological information of the investigated sites was available from earlier studies. In 2007 and 2008, Konz et al. (2010) measured surface runoff and soil water content at a plot on the south-facing hillslope (Fig. 1). On the north-facing hillslope, in-situ rain simulation experiments were performed on 1 m^2 plots on grassland sites in 2010 and 2011 to investigate overland flow on the plot scale (Fig. 1). The duration of each rain simulation was 1 h with an intensity of 36 mm h^{-1}. For a more detailed description of the measurement techniques, the reader is referred to Konz et al. (2010), Alaoui and Helbling (2006).

2.2.5. Topographic analysis

Topographic analysis of the hillslopes was performed with a digital elevation model with a cell size of 2 × 2 m (Swisstopo). Accuracy in X, Y and Z direction is ±0.5 m (1σ) in open terrain. We used the geographic information system software SAGA GIS (version 2.1.0) to calculate the topographic wetness index as

$$TWI = \ln\frac{A}{\tan\beta}, \quad (12)$$

where A is the upslope area per unit contour length and tanβ is the local slope (Beven and Kirkby, 1979). The triangular multiple flow direction algorithm (Seibert and McGlynn, 2007) was used to

calculate the upslope area. The TWI can be used to gain information on potential spatial soil moisture patterns and hydrological flow paths, related to the topography of the investigated site (Moore et al., 1991).

3. Results

3.1. Physical and hydrological soil properties

Sampled soils across the Urseren Valley are dominated by sand (50 ± 13%) and silt fractions (41 ± 9%) whereas the clay fraction plays a minor role (9 ± 5%) (n = 106) (Gysel, 2010 and own data). The texture classes according to Soil Survey Division Staff (1993) of the sampled depth profiles from the two hillslopes are given in Table 1. Highly fractured and weathered stone fragments of up to 0.3 m length within the soils have been observed at our sites. Skeleton content in the soils ranged from 1% to 45% dry weight (dw) with a mean of 20% dw (n = 100) on the north-facing slopes and from 3% to 65% dw with a mean of 19% dw (n = 28) on the south-facing slopes (Konz et al., unpublished data).

Saturated hydraulic conductivity (K_{sat}) ranged from 2.3×10^{-6} to 2.4×10^{-4} m s^{-1} with a harmonic mean of 1.1×10^{-5} m s^{-1} (n = 24) over both depth intervals in soils from the north-facing hillslope near the rain simulation experiments (Fig. 1 and Section 2.2.4). K_{sat} can be classified as moderately high to high according to the Soil Survey Division Staff (1993) and precipitation can therefore quickly pass the upper soil layers and percolate towards deeper soil zones. This is supported by the results from the rain simulation experiments at the north facing hillslope. During these experiments, surface runoff was absent or low at all sites, resulting in low runoff coefficients (RC) of 0–0.1 (RC = total surface runoff in mm/total precipitation in mm).

3.2. Air temperature, precipitation and its $\delta^{18}O$ values

Mean daily air temperature strongly varied between seasons and ranged from −16.2 to +19.8 °C (Fig. 2, top). Mean monthly precipitation was 98 ± 55 mm between September 2009 and June 2011 (MeteoSwiss, 2013). Measured (weekly and biweekly) $\delta^{18}O$ signals in precipitation strongly varied seasonally and ranged from −24.7 to −2.9‰ (Fig. 2, bottom). The volume weighted mean $\delta^{18}O$ value in precipitation at the north-facing hillslope was −13‰. The precipitation sample with a $\delta^{18}O$ value of −24.7‰ (Fig. 2) represents freshly fallen snow at the beginning of the winter season. The depth integrating bulk snow samples from March 2011 had a mean $\delta^{18}O$ value of −17.7 ± 1.9‰ (±standard deviation). The depth integrating bulk snow samples from May 2011 of a south-facing slope at 2400 m a.s.l. (about 8 km west from the investigated hillslope) had a mean $\delta^{18}O$ value of −17.6 ± 0.4‰ (n = 5). We therefore used these measured $\delta^{18}O$ values of snow as input data for the south-facing hillslope. This was considered a feasible approach, comparing our spatially distributed stable isotope data of snow (data not shown) and the fact that aspect had a minor influence on stable isotope values of snow in a study conducted by Dietermann and Weiler (2013) in the Swiss Alps.

The calculated daily $\delta^{18}O$ signals in precipitation strongly varied between seasons ranging from −28‰ in winter to −2.5‰ in summer (Fig. 2). The measured $\delta^{18}O$ values of precipitation were reproduced by the calculated daily $\delta^{18}O$ values of precipitation with a coefficient of determination of r^2 = 0.64 (p < 0.0001).

Table 1
Soil texture classes of the sampled depth profiles from the north- and south-facing hillslope according to Soil Survey Division Staff (1993).

Profile no.	Hillslope	0–0.3 m depth	>0.3 m depth
1	S	Silt loam	Silt loam
2, 5	S	Sandy loam	Sandy loam
3	S	Silt loam	Silt loam
4	S	Silt loam	Sandy loam
5	S	Sandy loam	Sandy loam
6, 10, 11	S	Silt loam	Silty clay loam
7	S	Silt loam	Sandy clay loam
8, 9	S	Silt loam	Loam
12	S	Silt loam	Sandy loam
13 and 15 to 26	N	Silt loam	Sandy loam
14	N	Loamy sand	Sandy loam
27a, 27b	Flat site	Silt loam	Silt loam

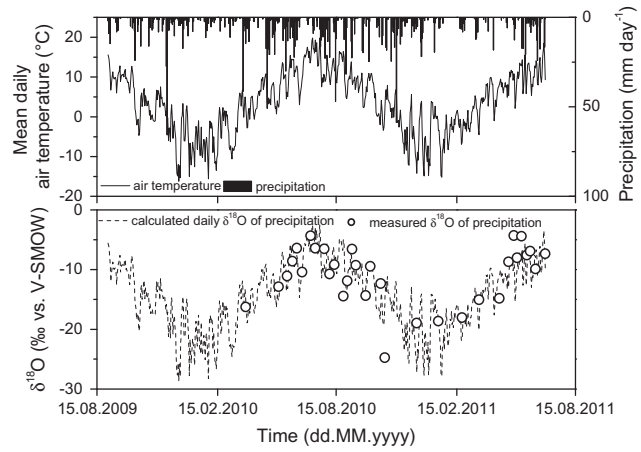

Fig. 2. Mean daily air temperature and daily precipitation volume at the MeteoSwiss station in Andermatt (upper panel, MeteoSwiss (2013)). Lower panel: measured (bi)weekly (summer) and monthly (winter) and calculated daily $\delta^{18}O$ values of precipitation. Calculated data was derived from correlation of $\delta^{18}O$ values of precipitation with air temperature. Summer precipitation was obtained as aggregate (bi)weekly samples and winter precipitation was obtained as monthly bulk snow samples.

3.3. Measured and simulated soil water $\delta^{18}O$ profiles

3.3.1. South-facing hillslope: measured $\delta^{18}O$ profiles

Most of the profiles at the south-facing hillslope (1, 2 and 4–12) have similar $\delta^{18}O$ depth distributions among each other (Fig. 3). Namely, we measured relatively higher $\delta^{18}O$ values close to the surface (−6 to −8‰), which decreased to about −11 to −12‰ in the deeper soil layers. The variability of $\delta^{18}O$ values decreased in the deeper soil layers (>0.3 m) and the strong seasonal variation of precipitation was reduced. The variability of $\delta^{18}O$ of soil water in the upper soil layers points to vertical percolation even at high slope angles. In the profiles 2 and 3 the coefficient of variation was clearly lower (CV = 1.5 and 0.9‰, Fig. 4) compared to the CV of the profiles 1 and 4–12, which ranged from about 1.7 to 2.8‰ (Fig. 4). Profile 3 had the lowest variability (CV = 0.9‰) and a dampened and attenuated $\delta^{18}O$ pattern. The topographic wetness index (TWI) was not correlated to the standard deviation of $\delta^{18}O$ of soil water within each profile (r^2 = 0.11). This is in contrast to the study of Garvelmann et al. (2012) who found a correlation of the TWI with the standard deviation of soil water stable isotopes (δ^2H) within the profiles.

The $\delta^{18}O$ value from winter precipitation of about −17.7‰ (depth integrating bulk snow samples from north-facing slopes across the Urseren Valley) was not detected in terms of a clear winter peak in the measured profiles. If we take fractionation processes during winter and the snowmelt period (e.g. Taylor et al., 2001) at the south-facing slopes into account, the lowest $\delta^{18}O$ value of soil water of about −14.5‰ of profile 1 at the south-facing hillslope could be regarded as representing the isotopically lighter

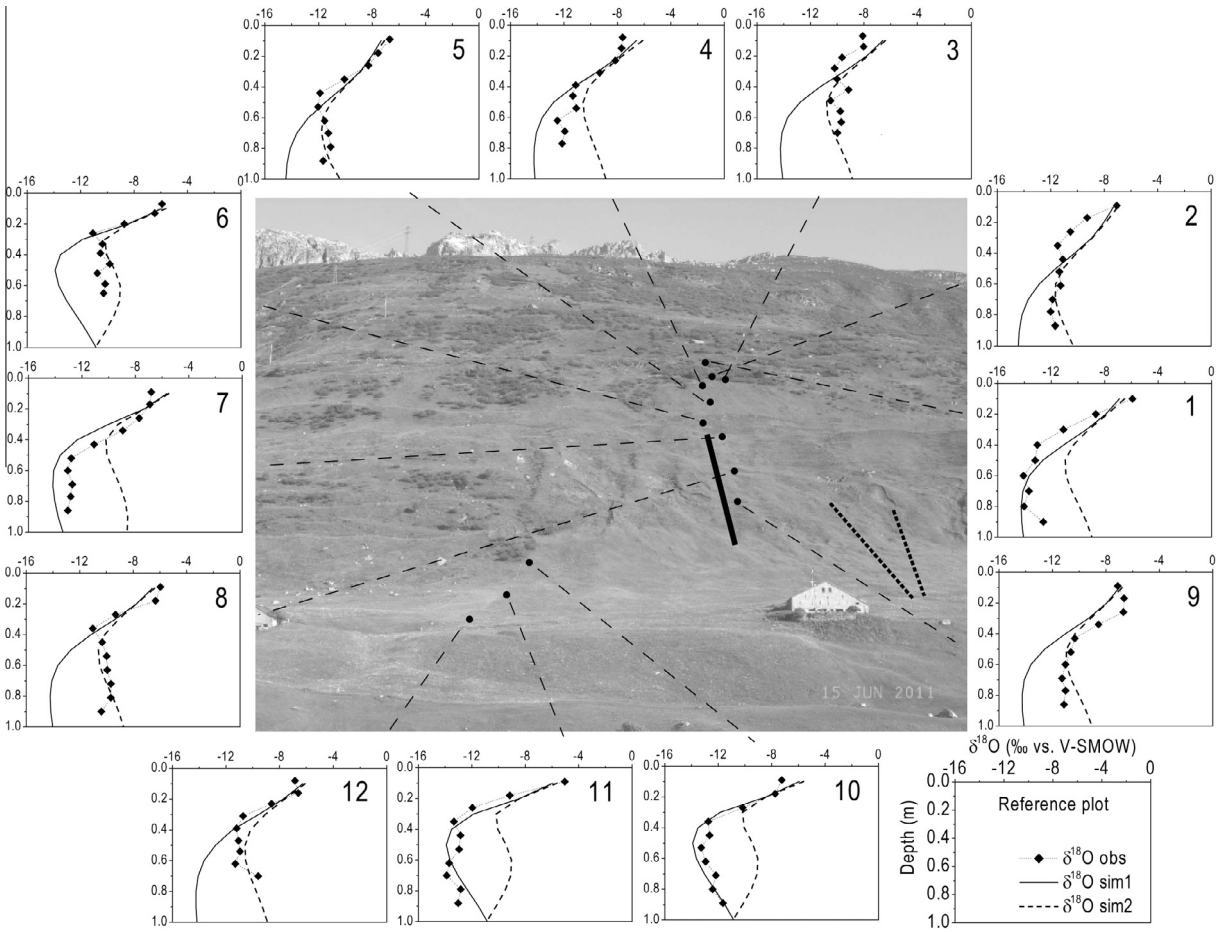

Fig. 3. Measured ("obs") and simulated ("sim") soil water $\delta^{18}O$ isotope profiles at the south-facing hillslope from June 2011. *X*-axes show $\delta^{18}O$ values of soil water from −16 to 0‰ and *y*-axes show depth from 0 to 1 m. Axes are the same for each plot. A reference plot with axes labels is shown. "sim1" refers to the model which includes snowmelt; "sim2" refers to the model which excludes snowmelt. Locations of the ERT profile (▬▬) and selected GPR profiles (▪▪▪▪▪▪) from the study of Carpentier et al. (2012) are also given.

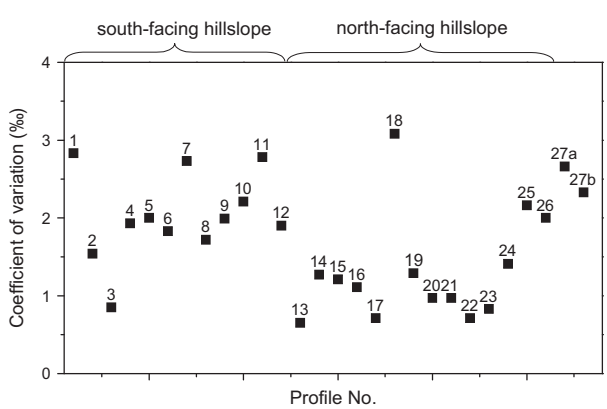

Fig. 4. Coefficient of variation of measured $\delta^{18}O$ of soil water profiles. Data labels indicate the number of the respective profile.

snowmelt component. Profiles with the lowest $\delta^{18}O$ value of about −10‰ suggest that the meltwater component was not present in these profiles. Precipitation volume of the period starting from snowmelt until the date of soil sampling in June 2011 was substantially lower (164 mm) than the amount of meltwater (approximately 284 mm snow water equivalent, SWE). We therefore expected the soil water $\delta^{18}O$ values in the lower horizon generally to be more negative in the case of a substantial contribution of snowmelt to the soil water pool. Possible explanations for the absent snowmelt peak in the $\delta^{18}O$ profiles will be discussed in detail below.

3.3.2. South-facing hillslope: simulated $\delta^{18}O$ profiles

$\delta^{18}O$ values of the simulated profiles ranged from −14.4‰ in the deeper soil layers to −5.5‰ in the upper soil layers (Fig. 3). Dispersivity λ was 0.02 m for all profiles, which is comparable to values of other soil hydrological studies (Pachepsky et al., 2004; van Genuchten and Wierenga, 1986; Vanderborght and Vereecken, 2007). The Nash–Sutcliffe efficiency coefficient (NSE) ranged from −11.9 (profile 3, Fig. 5) to 0.9 (profile 5, Fig. 5). If only the respective best fit (either data set "sim1" or "sim2") of each profile is considered, the median NSE is 0.73. Further, 83% of the simulated profiles have a NSE of 0.5 and above. The latter is considered as "satisfactory" according to Moriasi et al. (2007). The root mean squared errors (RMSE) ranged from 0.52‰ (profile 5, Fig. 6) to 3.18‰ (profile 11, Fig. 6). Application of the input data set without the snowmelt component ("sim2") reduced the RMSE of several simulated profiles. Taking only the respective best fit (either data set "sim1" or "sim2") of each profile into account, the average RMSE was 1.0 ± 0.3‰ (mean ± standard deviation). For the profiles 1, 7, 10 and 11 we were able to reproduce the measured profile with the input parameters "sim1", including the snowmelt component (Fig. 3). For the remaining profiles, the exclusion of the snowmelt component from the input ("sim2") could reduce the high deviation of about −4‰ of the simulated

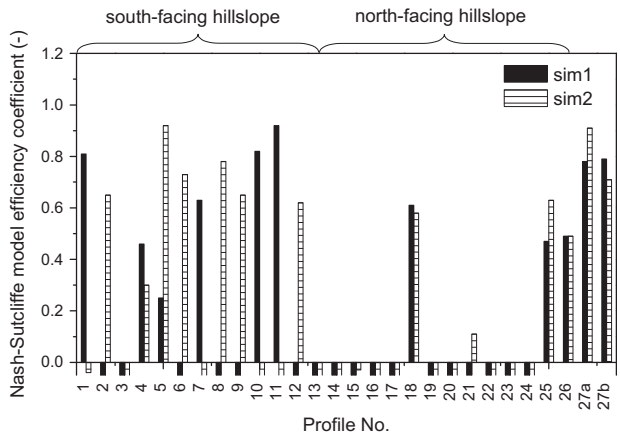

Fig. 5. Nash–Sutcliffe model efficiency coefficient (NSE) for simulated $\delta^{18}O$ of soil water profiles. Data labels indicate the number of the respective profile. "sim1" refers to the model which includes snowmelt; "sim2" refers to the model which excludes snowmelt. For reasons of clarity the *y*-axis (NSE) is scaled from −0.05 to 1.2.

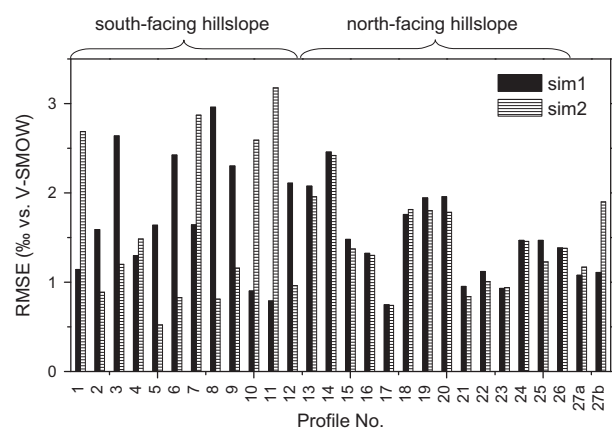

Fig. 6. Root mean squared error of simulated $\delta^{18}O$ soil water stable isotope profiles of the north- and south-facing hillslope. Data labels indicate the number of the respective profile. "sim1" refers to the model which includes snowmelt; "sim2" refers to the model which excludes snowmelt.

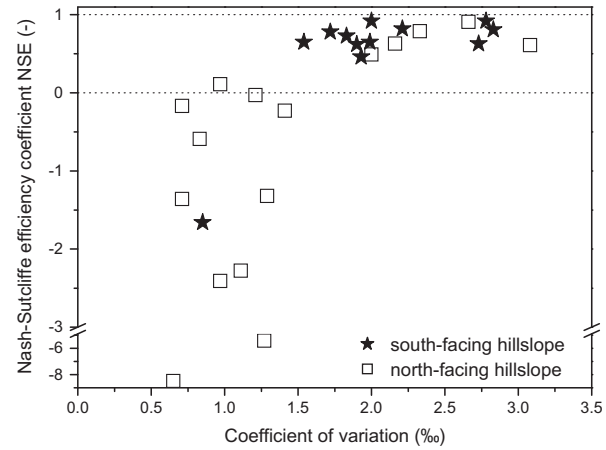

Fig. 7. Comparison of Nash–Sutcliffe model efficiency (NSE) to the coefficient of variation (CV). For orientation the dashed lines refer to NSE = 1 (simulated data match the observed data) and NSE = 0 (model simulations are as accurate as the mean of the observed data). Please note the break on the *y*-axis.

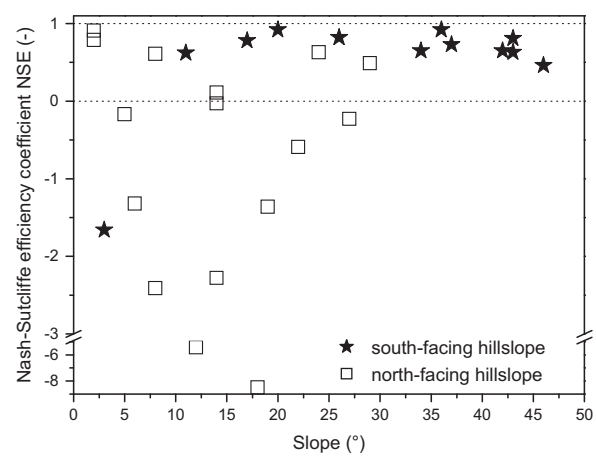

Fig. 8. Nash–Sutcliffe model efficiency (NSE) versus slope angle. For orientation, the dashed lines refer to NSE = 1 (simulated data match the observed data) and NSE = 0 (model simulations are as accurate as the mean of the observed data). Please note the break on the *y*-axis.

from the measured profiles. With this approach, it was possible to reproduce the measured profiles 2, 3, 5, 8, 9 and 12, in which the isotopically light winter precipitation seemed to be absent (Fig. 3). We also tested other input parameter sets (e.g. considering higher dispersivities), which however were not able to compensate for the mismatch of 4‰ between the simulated and the measured profiles (data not shown).

Comparing the NSE with the CV visualizes that the model only performs efficiently above a certain threshold of the CV (Fig. 7). Of course, a low model efficiency (NSE) for profiles with a low CV can be expected, since both parameters decrease with decreasing sum of squared deviations from the mean observed values. However, high variations of $\delta^{18}O$ values within a profile (high CV) can most likely be associated with vertical percolation.

For a wide range of slope angles at the south-facing hillslope, the NSE (considering the best fit; either "sim1" or "sim2") was between 0.46 and 1 (Fig. 8). This suggests that vertical percolation was not restricted to low slope angles. Even at a slope angle of about 46° the water can percolate vertically within the soil profile to deeper soil layers.

3.3.3. North-facing hillslope: measured $\delta^{18}O$ profiles

The measured profiles 18 and 25–27b were highly variable with depth, with a coefficient of variation (CV) of 1.4–3.1‰ (Figs. 9 and 4). The pattern of these profiles indicates a direct imprint of the temporal highly variable $\delta^{18}O$ values of incoming precipitation (Fig. 2). A second group with a relatively low variability (CV ⩽ 1.4‰), indicating redistribution and mixing of soil water from various precipitation events, comprises the profiles 14–17, 19, 20 and 24. Within this group the variability of $\delta^{18}O$ values clearly decreased with depth in some profiles (e.g. 14, 15, 19 and 20). Redistribution and mixing of water due to lateral subsurface flow of soil or groundwater can be an important process in the profiles 13–19 since a small stream passes about 10–20 m upslope to the profiles from right to left (Fig. 9). Profiles 21, 22 and 23 can be regarded as intermediate profiles of these groups. Even though their CV is only 0.7–1.0‰, their pattern was qualitatively similar to the profiles 24–27a, but strongly dampened. These different patterns highlight the spatial heterogeneity of soil hydrological processes at the hillslope scale. Like on the south-facing hillslope, the TWI was not correlated to the standard deviation of $\delta^{18}O$ of soil water within each profile on the north-facing hillslope (r^2 = 0.01).

On the second sampling day (5 August 2010, profiles 22–27a), there were about 20 mm of rainfall with a $\delta^{18}O$ value of −10.4‰, whereas the rainfall of the 5 preceding days (22 mm) had a more positive $\delta^{18}O$ value of −6.9‰. The imprint of the rainfall from 5

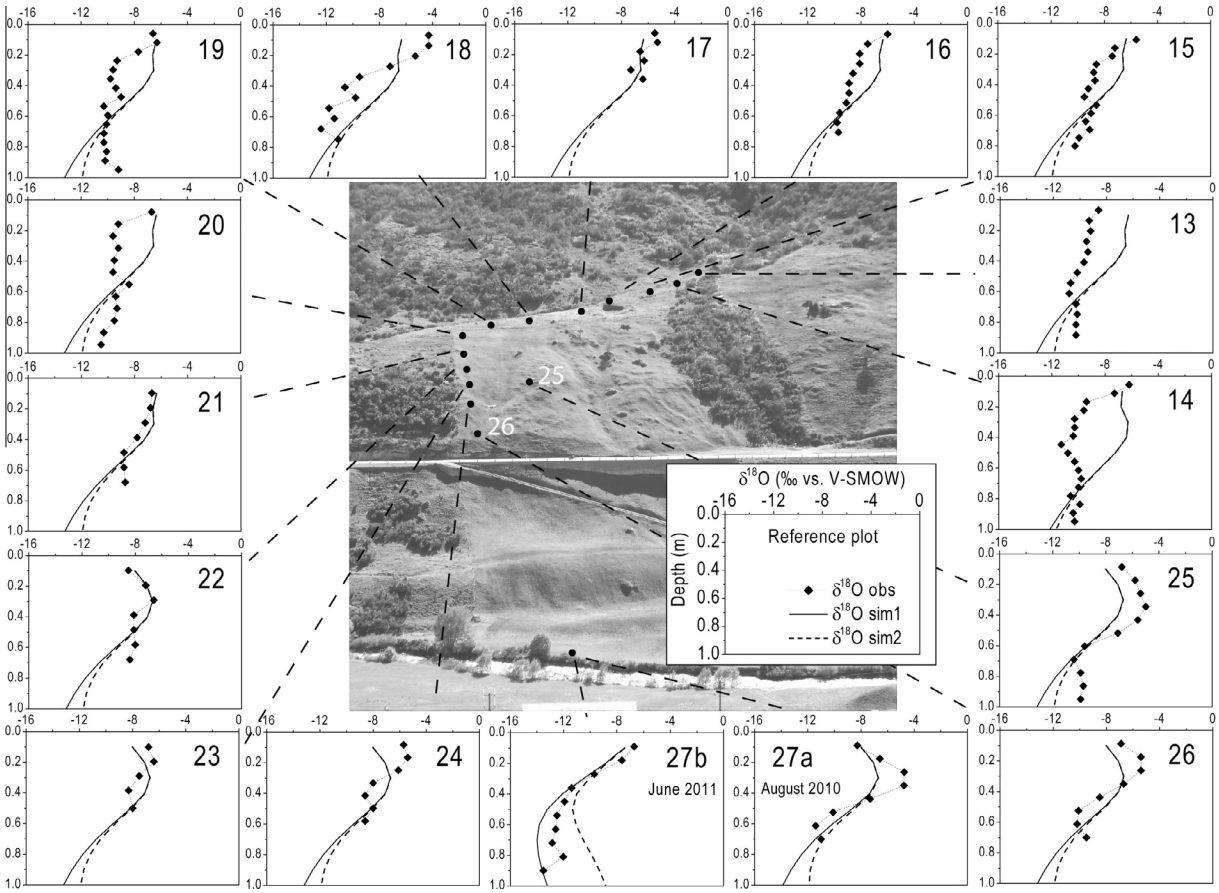

Fig. 9. Measured ("obs") and simulated ("sim") $\delta^{18}O$ values of soil water stable isotope profiles at the north-facing hillslope from August 2010. *X*-axes show $\delta^{18}O$ of soil water from −16 to 0‰, *y*-axes show depth from 0 to 1 m. A reference plot with axes labels is shown. Plots 27a and 27b show the profiles from the same site taken in August 2010 and June 2011, respectively. "sim1" refers to the simulation run which includes snowmelt; "sim2" refers to the simulation run which excludes snowmelt.

August 2010 was visible in the profiles 22–27a (Fig. 9), which tend to "bend" to more negative values $\delta^{18}O$ values in the upper 0.1 m interval compared to the profiles 13–21. There was no significant difference ($p = 0.35$) in the CV between the profiles taken on the first day (4 August 2010, profiles 13–21) and the profiles taken on the second day (5 August 2010, profiles 22–27a).

For plots 27a and 27b of Fig. 9, the same site was sampled in August 2010 and June 2011, respectively. The distinct $\delta^{18}O$ summer peak of about −4.5‰ of profile 27a was not visible in the deeper soil layers of profile 27b, taken 10 months later. Assuming only vertical percolation at this site, the diverse patterns of these two profiles indicate that soil water was replaced in the upper 1 m at least within one year.

No clear winter peak was detected in the $\delta^{18}O$ profiles at the north-facing hillslope, and the ratios were more positive than the annual average in precipitation (−13‰). This suggests that the transit time of soil water in the upper 1 m was eventually shorter than 4 months, which is the approximate time span from snowmelt to the sampling date.

3.3.4. North-facing hillslope: simulated $\delta^{18}O$ profiles

The two simulation input sets "sim1" and "sim2" yielded similar profiles, which only deviated slightly from each other in the lower soil layers (Fig. 9). This was supported by the similar root mean squared error (RMSE, Fig. 6) and Nash–Sutcliffe model efficiency (NSE, Fig. 5) for each respective profile. The small differences between the profiles simulated with "sim1" and "sim2" indicate a low potential and de facto influence of snowmelt at that sampling date in the year (4 and 5 August 2010 on the north-facing hillslope). At the north-facing hillslope, only the profiles 18, 21, 25, 26, and 27a and 27b had a NSE > 0. The mean RMSE for the respective best fits of all profiles from this hillslope was 1.4 ± 0.5‰. The distinct simulated $\delta^{18}O$ peak of about −6‰ at 0.4 m depth was observed in profiles 22, 25 and 27a, but the variability of the simulated profiles was more dampened.

The poor reproduction of measured isotope profiles 13–17, 19, 20, 22, 23 and 24 by the simulations (NSE < 0, Fig. 5) indicates that vertical percolation is not the dominant water flow process at these sites, at least in the lower soil layers below 0.2 m depth. The simulated $\delta^{18}O$ values in the upper 0.1 m interval matched the measured values at least for the profiles 14, 16, 19, 21 and 22. Comparing the neighboring profiles 21 (taken on 4 August 2010) and 22 (taken on 5 August 2010) suggests that the applied model was able to reproduce the $\delta^{18}O$ values of soil water induced by the infiltration of rainfall on 5 August 2010. We consider the impact of the rainfall event of minor importance for the overall $\delta^{18}O$ patterns in the deeper soil layers, which is supported by the applied model using daily time steps.

Comparison of the NSE and the CV for the north-facing hillslope supports the findings from the south-facing hillslope (Fig. 7). Above a threshold of the CV of about 1.5‰ (Fig. 7) the model performed more efficient than for profiles with a CV < 1.5‰. In other words, vertical percolation was most likely dominant in profiles with a CV > 1.5‰. Further, a NSE > 0.49 was found for profiles at low and at high slope angles of the north-facing hillslope (Fig. 8). This suggests that vertical percolation within the soil profile was not restricted to low slope angles.

4. Discussion

4.1. Physical and hydrological soil properties

Similar to our results from the rain simulation experiments, fast and nearly complete infiltration was observed at the south facing hillslope in an earlier study under natural rainfall conditions (Konz et al., 2010). The authors found that soil water content in 0.10–0.35 m below ground quickly responded to incoming precipitation (Fig. 7 of Konz et al. (2010)). The reaction to precipitation inputs often started within 10 min in 0.35 m and it was often several hours faster in 0.35 m than in 0.10 m depth (data not shown). Additionally, the absolute change in volumetric soil water content was higher 0.35 m than in 0.10 m depth. This can be indicative for preferential vertical percolation and bypass flow. Only small amounts of surface runoff of 0–3.5 mm per month were detected during April to November 2007 and the runoff coefficient was only 0.02 for the observation period from April to November 2007 (Konz et al. (2010); precipitation volume during this period was comparable to our observation period). Furthermore, Scherrer (1996) studied runoff generation processes in rain simulation experiments very near to our sites at the south-facing hillslope and he showed that preferential bypass flow can occur at these sites. He associated the preferential bypass flow to animal burrows, which he observed in soil profiles and soil trenches. Our soil physical and hydrological data are in accordance with the study of Carpentier et al. (2012), who state that the overlaying soil material in the Urseren Valley allows fast drainage of water.

4.2. Subsurface water pathways as indicated by $\delta^{18}O$ depth profiles

Gazis and Feng (2004) investigated stable isotopes of soil water at sites with comparable climate (which influences temporal dynamics of stable isotopes in precipitation) and soil characteristics (e.g. texture). They found vertical subsurface flow to be important at their sites, which they inferred from abrupt changes in the stable isotope profile with depth. These changes can be produced by successive precipitation events with distinct stable isotope signatures if infiltrating precipitation pushes "old" soil pore water downward (e.g. Klaus et al., 2013). In our study, distinct $\delta^{18}O$ peaks from snowmelt and summer precipitation were identified in several investigated soil profiles. The relatively high variability (CV > 1.5‰) of $\delta^{18}O$ of soil water in several measured profiles combined with a "satisfactory" model efficiency (NSE > 0.5) for the respective simulated profiles point to vertical percolation and stable isotope transport within the soil profile even at high slope angles of up to 46° (Figs. 4 and 8). Hence, vertical percolation can predominate over other flow processes (e.g. lateral subsurface flow) at certain positions on a steep hillslope. In case of a permeable bedrock layer (like in the Urseren Valley), the water can subsequently be routed directly to deeper zones and recharge into the bedrock. Since a larger volume of bedrock is available for water storage in steep watersheds (Sayama et al., 2011), a vertical percolation within a drainable soil can therefore be hydrologically even more important for recharge into bedrock in mountainous headwater catchments compared to watersheds with a smooth topography. Vertical structures at the south-facing hillslope in the Urseren Valley, which Carpentier et al. (2012) interpreted as faults/fractures or vertically dipping layers, supports infiltration of water into deeper zones of the bedrock.

Nevertheless, there were also profiles at the investigated hillslopes in which the $\delta^{18}O$ peaks from snowmelt or summer precipitation were strongly dampened and the variability of $\delta^{18}O$ values within a soil profile was relatively low (CV < 1.5‰). For strongly dampened $\delta^{18}O$ profiles at the north-facing hillslope, the applied one-dimensional model using the Richards equation coupled with the advection–dispersion equation was not able to reproduce the measured $\delta^{18}O$ values of soil water, even on relatively flat sites (Figs. 7 and 8). Processes like lateral subsurface flow, mixing of waters, the influence of groundwater, and/or highly dispersive transport can reduce the variability in the deeper layers resulting in constant isotope signatures with depth (Barnes and Turner, 1998; Garvelmann et al., 2012; Gazis and Feng, 2004; Gehrels et al., 1998; Stumpp and Hendry, 2012). In the study of Garvelmann et al. (2012), profiles with a low variability of soil water stable isotopes – interpreted as indication of lateral subsurface flow – had a high TWI. This indicated accumulation of water at the respective site in their study. The authors therefore used the TWI to infer information on subsurface hydrological processes. In contrast, in our study the TWI is not correlated to the standard deviation of $\delta^{18}O$ of soil water within each profile. This points to decoupling of subsurface and surface water flow patterns at our sites. We conclude that information on subsurface hydrology cannot necessarily be obtained by only using the TWI at our sites.

Furthermore, the simulations revealed spatially heterogeneous snowmelt inputs into the soils. Several (interacting) processes, which would need further investigations, might act at our sites. The absent $\delta^{18}O$ value of the meltwater in the soil profiles can be partially explained by preferential subsurface flow of meltwater, which bypasses the soil layer and subsequently recharges into the bedrock (Brooks et al., 2010; Buttle and Sami, 1990; Darling and Bath, 1988; Gehrels et al., 1998; Stewart and McDonnell, 1991). The rock fragments of up to 0.3 m at our sites can promote funneling of water flow along their walls, which increases water flow velocity (Bogner et al., 2008) and results in fast water transport to deeper soil layers. Further, preferential flow within partially frozen soils might occur (Lundin and Johnsson, 1994; Stähli et al., 1996). Preferential bypass flow might also be explained by animal burrows (mice) which have been frequently observed visually at the soil surface of our sites after snowmelt (see photo 1 in the supplementary data). Furthermore, surface runoff of meltwater over frozen (Granger et al., 1984) or water saturated soils (infiltration/saturation excess overland flow) can lead to a low fraction of infiltrating meltwater. Surface runoff during the snowmelt periods was not quantitatively determined at our sites but it was observed visually during field campaigns in early spring at the onset of snowmelt (see photo 2 in the supplementary data). Soil temperatures at our sites can decrease to 0 °C during winter (data not shown) promoting possible surface runoff of meltwater over these frozen soils. Spatial heterogeneous snowmelt inputs were also observed in studies of Litaor et al. (2008) and Williams et al. (2009). They were mostly associated to redistribution of snow by wind or spatially variable melt patterns controlled by elevation, aspect and vegetation. Spatial snow redistribution due to avalanches was frequently observed at our sites and might further enhance spatially heterogeneous snowmelt inputs into the soils (see photo 3 in the supplementary data).

We propose a conceptual flow model, which can be used to understand the main flow processes in this study (Fig. 10). The comparison of measured and simulated $\delta^{18}O$ profiles can be used as a diagnostic tool for a relatively quick characterization of spatial heterogeneity of water inputs into the soil and transport processes at the hillslope scale. For highly permeable soils with low dispersivities like in our study, we suggest two main classes of $\delta^{18}O$ profiles that can be observed (profiles A1–A3 versus profile B in Fig. 10). In regions with seasonally varying $\delta^{18}O$ values in precipitation, a preservation of this variability in the $\delta^{18}O$ values in the soil water indicates vertical percolation within the soil (profiles A1–A3 in Fig. 10). Profile A3 in Fig. 10 still implies vertical percolation, even if the $\delta^{18}O$ value of snowmelt water is absent. The latter was inferred from the simulated profiles using different input parameters. The second class is represented by profile B in Fig. 10, which has a nearly constant $\delta^{18}O$ value of soil water with

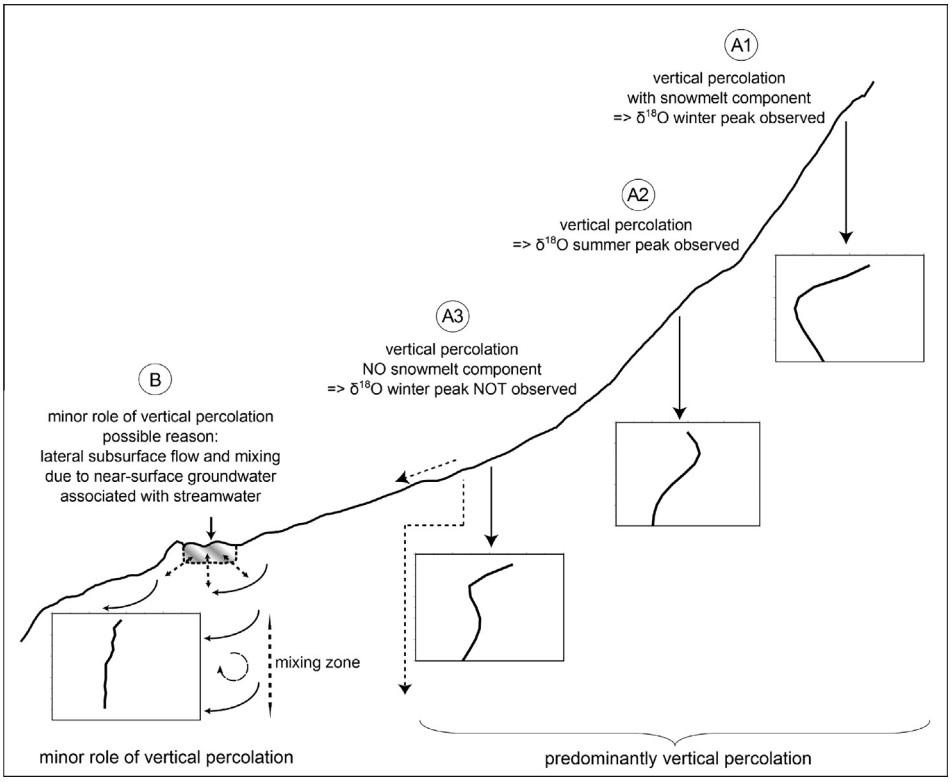

Fig. 10. Conceptual subsurface water flow model. See text for detailed explanations.

Table 2
Classification of the measured $\delta^{18}O$ soil water profiles (profile numbers are given) according to the conceptual flow model of Fig. 10.

Schematic profile A1	Schematic profile A2	Schematic profile A3	Schematic profile B
1	18	2	13
4	24	3	14
7	25	5	15
10	26	6	16
11	27a	8	17
27b		9	19
		12	20
			21
			22
			23

depth. The latter suggests a minor role of vertical percolation and a stronger influence of, for example, lateral subsurface flow, which can be due to near-surface groundwater flow in the vicinity of streams (Fig. 10) or if recharge to the bedrock is hampered. Classification of our measured profiles (1–27b) according to the suggested conceptual model (Fig. 10) is given in Table 2. 64% of the profiles correspond to type A profiles, indicating a predominant role of vertical percolation within these soils.

5. Conclusion

The temporal high variation of $\delta^{18}O$ values in precipitation and its subsequent attenuation in soil pore water was successfully used to track the water flow in the unsaturated zone and to estimate the relative importance of vertical percolation versus lateral subsurface flow in two steep subalpine hillslopes. In some profiles, $\delta^{18}O$ values of soil pore water indicate fast infiltration into the soil layers and subsequent vertical percolation into deeper zones even at steep slopes. This is supported by physical soil data (sandy soil texture and high skeleton contents) and surface runoff measurements during rain simulations. The high infiltration capacity can be explained by the relatively high values of K_{sat}, which we measured at selected undisturbed soil samples in the laboratory. Overland flow during summer rain events, which can cause sheet erosion of soil, therefore plays a minor role in our study area. The vertical transport processes were confirmed by a one-dimensional soil physical model coupled with the advection–dispersion equation, which was used to simulate the measured $\delta^{18}O$ profiles. In other profiles, however, the $\delta^{18}O$ values of soil pore water also suggest that processes, like for example lateral subsurface flow or mixing of water occurred at the investigated sites, which was most likely due to near-surface groundwater at one hillslope. Non-equilibrium flow processes can lead to poor model performance, since the applied model is at the present stage designed for uniform equilibrium flow and transport. Furthermore, the model simulations suggest a spatial heterogeneity of snowmelt input into the soils at the hillslope scale.

The applied soil sampling and stable isotope analysis proved to be a fast (one single sampling campaign) and suitable approach to investigate actual soil water flow paths at steep subalpine hillslopes. Within 1–2 days of sampling and 3 days of soil water stable isotope measurements only, we were able to generate a quick time-integrating overview of subsurface hydrological processes at the hillslope scale. In combination with a physically based soil model, we suggest this method as a tool to investigate hillslope hydrology at sites were more conventional soil moisture equipment cannot be easily installed (e.g. in stony soils or during harsh winter conditions) or if time is a limiting factor.

Acknowledgements

We would like to thank Barbara Herbstritt, Benjamin Gralher, and Jakob Garvelmann for their great support and background information during stable isotopes measurements at the laboratory

of the Chair of Hydrology, University of Freiburg, Germany. We also would like to thank Björn Probst and Gregor Juretzko for their assistance during soil sampling in the field and Marianne Caroni for soil texture analyses. Susanne Lagger and Philipp Schmidt are kindly acknowledged for their help during the irrigation experiments and we thank Silvia Hunkeler for measuring saturated hydrologic conductivity of soil samples. Finally, we would like to thank the three anonymous reviewers for their constructive comments, which greatly helped to improve our manuscript. Peter K. Kitanidis is gratefully acknowledged for handling the review process.

This work was part of the project "The ecological and socio-economic consequences of land transformation in alpine regions: an interdisciplinary assessment and VALuation of current changes in the Urseren Valley, key region in the Swiss central Alps", funded by the Swiss National Science Foundation (SNF), grant no. CR30I3_124809. (The SNF was not involved in study design; in the collection, analysis and interpretation of data; and in the writing of the report.)

Appendix A. Supplementary material

Supplementary data associated with this article can be found, in the online version, at http://dx.doi.org/10.1016/j.jhydrol.2014.07.031.

References

Adomako, D., Maloszewski, P., Stumpp, C., Osae, S., Akiti, T.T., 2010. Estimating groundwater recharge from water isotope (delta H-2, delta O-18) depth profiles in the Densu River basin, Ghana. Hydrol. Sci. J. – J. Des Sci. Hydrol. 55 (8), 1405–1416.

Alaoui, A., Helbling, A., 2006. Evaluation of soil compaction using hydrodynamic water content variation: comparison between compacted and non-compacted soil. Geoderma 134 (1–2), 97–108.

Asano, Y., Uchida, T., Ohte, N., 2002. Residence times and flow paths of water in steep unchannelled catchments, Tanakami, Japan. J. Hydrol. 261 (1–4), 173–192.

Bachmair, S., Weiler, M., 2011. New dimensions of hillslope hydrology. In: Levia, D.F., Carlyle-Moses, D., Tanaka, T. (Eds.), Forest Hydrology and Biogeochemistry: Synthesis of Past Research and Future Directions. Ecological Studies. Springer, Netherlands, pp. 455–481.

Barnes, C.J., Allison, G.B., 1988. Tracing of water-movement in the unsaturated zone using stable isotopes of hydrogen and oxygen. J. Hydrol. 100 (1–3), 143–176.

Barnes, C.J., Turner, J.V., 1998. Isotopic exchange in soil water. In: Kendall, C., McDonnell, J.J. (Eds.), Isotope Tracers in Catchment Hydrology. Elsevier Science, Amsterdam, pp. 137–163.

Beven, K.J., 1986. Hillslope runoff processes and flood frequency characteristics. In: Abrahams, A.D. (Ed.), Hillslope Processes. Allen and Unwin, Boston, pp. 187–202.

Beven, K., Germann, P., 2013. Macropores and water flow in soils revisited. Water Resour. Res. 49 (6), 3071–3092.

Beven, K.J., Kirkby, M.J., 1979. A physically based, variable contributing area model of basin hydrology/un modèle à base physique de zone d'appel variable de l'hydrologie du bassin versant. Hydrol. Sci. Bull. 24 (1), 43–69.

Bogner, C., Engelhardt, S., Zeilinger, J., Huwe, B., 2008. Visualization and analysis of flow patterns and water flow simulations in disturbed and undisturbed tropical soils. In: Beck, E., Bendix, J., Kottke, I., Makeschin, F., Mosandl, R. (Eds.), Gradients in a Tropical Mountain Ecosystem of Ecuador. Ecological Studies: Analysis and Synthesis, pp. 387–396.

Brooks, J.R., Barnard, H.R., Coulombe, R., McDonnell, J.J., 2010. Ecohydrologic separation of water between trees and streams in a Mediterranean climate. Nat. Geosci. 3 (2), 100–104.

Buttle, J.M., Sami, K., 1990. Recharge processes during snowmelt – an isotopic and hydrometric investigation. Hydrol. Process. 4 (4), 343–360.

Carpentier, S. et al., 2012. Geophysical imaging of shallow subsurface topography and its implication for shallow landslide susceptibility in the Urseren Valley, Switzerland. J. Appl. Geophys. 83, 46–56.

Coppola, A. et al., 2013. Measuring and modeling water content in stony soils. Soil Tillage Res. 128, 9–22.

Darling, W.G., Bath, A.H., 1988. A stable isotope study of recharge processes in the English chalk. J. Hydrol. 101 (1–4), 31–46.

Dietermann, N., Weiler, M., 2013. Spatial distribution of stable water isotopes in alpine snow cover. Hydrol. Earth Syst. Sci. 17 (7), 2657–2668.

Dobriyal, P., Qureshi, A., Badola, R., Hussain, S.A., 2012. A review of the methods available for estimating soil moisture and its implications for water resource management. J. Hydrol. 458, 110–117.

Dunne, T., 1978. Field studies of hillslope flow processes. In: Kirkby, J. (Ed.), Hillslope Hydrology. Wiley, London, pp. 227–293.

Dusek, J., Vogel, T., Sanda, M., 2012. Hillslope hydrograph analysis using synthetic and natural oxygen-18 signatures. J. Hydrol. 475, 415–427.

Freer, J. et al., 2002. The role of bedrock topography on subsurface storm flow. Water Resour. Res. 38 (12).

Fry, B., 2003. Steady state models of stable isotopic distributions. Isot. Environ. Health Stud. 39 (3), 219–232.

Garvelmann, J., Külls, C., Weiler, M., 2012. A porewater-based stable isotope approach for the investigation of subsurface hydrological processes. Hydrol. Earth Syst. Sci. 16 (2), 631–640.

Gazis, C., Feng, X.H., 2004. A stable isotope study of soil water: evidence for mixing and preferential flow paths. Geoderma 119 (1–2), 97–111.

Gehrels, J.C., Peeters, J.E.M., De Vries, J.J., Dekkers, M., 1998. The mechanism of soil water movement as inferred from O-18 stable isotope studies. Hydrol. Sci. J. – J. Des Sci. Hydrol. 43 (4), 579–594.

Gonfiantini, R., 1986. Environmental isotopes in lake studies. In: Fritz, P., Fontes, J.C. (Eds.), Handbook of Environmental Isotope Geochemistry, vol. 2: The Terrestrial Environment. Elsevier Scientific Publishing Company, Amsterdam, pp. 113–168.

Granger, R.J., Gray, D.M., Dyck, G.E., 1984. Snowmelt infiltration to frozen prairie soils. Can. J. Earth Sci. 21 (6), 669–677.

Gysel, A., 2010. GIS-gestützte Modellierung der Kohlenstoffkonzentration, der Korngrössen und des Bodentyps mit multipler Regression, Ordinary Kriging und Random Forest in einem alpinen Tal (Urserntal, Schweiz). Masters Thesis, University of Basel, Basel, Switzerland, p. 144.

Hargreaves, G., Samani, Z., 1982. Estimating potential evapotranspiration. J. Irrigation Drainage Div. 108, 225–230.

Hopp, L., McDonnell, J.J., 2009. Connectivity at the hillslope scale: identifying interactions between storm size, bedrock permeability, slope angle and soil depth. J. Hydrol. 376 (3–4), 378–391.

Ingraham, N.L., Shadel, C., 1992. A comparison of the toluene distillation and vacuum/heat methods for extracting soil water for stable isotopic analysis. J. Hydrol. 140 (1–4), 371–387.

IUSS Working Group WRB, 2006. World Reference Base for Soil Resources: A Framework for International Classification, Correlation and Communication. Food and Agriculture Organization of the United Nations, Rome, p. 128.

Jadoon, K.Z. et al., 2012. Estimation of soil hydraulic parameters in the field by integrated hydrogeophysical inversion of time-lapse ground-penetrating radar data. Vadose Zone J. 11 (4).

Kägi, H.U., 1973. Die traditionelle Kulturlandschaft im Urserental; Beitrag zur alpinen Kulturgeographie. PhD Thesis, University of Zürich, Zürich, Switzerland, p. 211.

Klaus, J., Zehe, E., Elsner, M., Kuells, C., McDonnell, J.J., 2013. Macropore flow of old water revisited: experimental insights from a tile-drained hillslope. Hydrol. Earth Syst. Sci. 17 (1), 103–118.

Klute, A., Dirksen, C., 1986. Hydraulic conductivity and diffusivity: laboratory methods. In: Klute, A. (Ed.), Methods of Soil Analysis: Part 1 – Physical and Mineralogical Methods. American Society of Agronomy, Madison, Wisconsin, pp. 687–734.

König, N., 2009. Handbuch Forstliche Analytik: Eine lose Blattsammlung der Analysemethoden im Forstbereich. Bundesministerium für Verbraucherschutz, Ernährung und Landwirtschaft, p. 568.

Konz, N., Baenninger, D., Konz, M., Nearing, M., Alewell, C., 2010. Process identification of soil erosion in steep mountain regions. Hydrol. Earth Syst. Sci. 14 (4), 675–686.

Körner, C., Wieser, G., Cernusca, A., 1989. Der Wasserhaushalt waldfreier Gebiete in den österreichischen Alpen zwischen 600 und 2600 m Höhe. In: Cernusca, A. (Ed.), Struktur und Funktion von Graslandökosystemen im Nationalpark Hohe Tauern. Wagner, Innsbruck, Austria, pp. 119–153.

Küttel, M., 1990. Der subalpine Schutzwald im Urserental – ein inelastisches Oekosystem. Bot. Helv. 100/2 (2).

Labhart, T.P., 1977. Aarmassiv und Gotthardmassiv. Sammlung Geologischer Führer. Borntraeger, Berlin.

Lindenmaier, F., Zehe, E., Dittfurth, A., Ihringer, J., 2005. Process identification at a slow-moving landslide in the Vorarlberg Alps. Hydrol. Process. 19 (8), 1635–1651.

Linsley, K., 1943. A simple procedure for the day-to-day forecasting of runoff from snow-melt. Trans. – Am. Geophys. Union 24, 62–67.

Litaor, M.I., Williams, M., Seastedt, T.R., 2008. Topographic controls on snow distribution, soil moisture, and species diversity of herbaceous alpine vegetation, Niwot Ridge, Colorado. J. Geophys. Res. – Biogeosci. 113 (G2).

Lundin, L.C., Johnsson, H., 1994. Ion dynamics of a freezing soil monitored in-situ by time-domain reflectometry. Water Resour. Res. 30 (12), 3471–3478.

Lunt, I.A., Hubbard, S.S., Rubin, Y., 2005. Soil moisture content estimation using ground-penetrating radar reflection data. J. Hydrol. 307 (1–4), 254–269.

Lv, M., Hao, Z., Liu, Z., Yu, Z., 2013. Conditions for lateral downslope unsaturated flow and effects of slope angle on soil moisture movement. J. Hydrol. 486, 321–333.

Majoube, M., 1971. Fractionement en oxygen-18 et en deuterium entre l'eau et sa vapeur. J. Chim. Phys. – Chim. Biol. 68 (10), 1423–1436.

McConville, C., Kalin, R.M., Johnston, H., McNeill, G.W., 2001. Evaluation of recharge in a small temperate catchment using natural and applied delta O-18 profiles in the unsaturated zone. Ground Water 39 (4), 616–623.

McDonnell, J.J., Stewart, M.K., Owens, I.F., 1991. Effect of catchment-scale subsurface mixing on stream isotopic response. Water Resour. Res. 27 (12), 3065–3073.

Menzel, L., 1997. Modellierung der Evapotranspiration im System Boden-Pflanze-Atmosphäre. PhD Thesis, ETH Zürich, Zürich, Switzerland, p. 128.
MeteoSwiss, 2013. IDAweb the data portal of MeteoSwiss for research and teaching. Federal Office Meteorology Climatology.
Meusburger, K., Alewell, C., 2008. Impacts of anthropogenic and environmental factors on the occurrence of shallow landslides in an alpine catchment (Urseren Valley, Switzerland). Nat. Hazards Earth Syst. Sci. 8 (3), 509–520.
Moore, I.D., Grayson, R.B., Ladson, A.R., 1991. Digital terrain modelling: a review of hydrological, geomorphological, and biological applications. Hydrol. Process. 5 (1), 3–30.
Moriasi, D.N. et al., 2007. Model evaluation guidelines for systematic quantification of accuracy in watershed simulations. Trans. Asabe 50 (3), 885–900.
Mualem, Y., 1976. New model for predicting hydraulic conductivity of unsaturated porous-media. Water Resour. Res. 12 (3), 513–522.
Nash, J.E., Sutcliffe, J.V., 1970. River flow forecasting through conceptual models part I — a discussion of principles. J. Hydrol. 10 (3), 282–290.
Pachepsky, Y.A., et al., 2004. Reality and fiction of models and data in soil hydrology. In: Feddes, R.A., DeRooij, G.H., VanDam, J.C. (Eds.), Unsaturated-Zone Modeling: Progress, Challenges and Applications, pp. 231–260.
Penna, D., Borga, M., Norbiato, D., Fontana, G.D., 2009. Hillslope scale soil moisture variability in a steep alpine terrain. J. Hydrol. 364 (3–4), 311–327.
Renger, M. et al., 2009. Ergebnisse und Vorschläge der DBG-Arbeitsgruppe "Kennwerte des Bodengefüges" zur Schätzung bodenphysikalischer Kennwerte. In: Wessolek, G., Kaupenjohann, M., Renger, M. (Eds.), Bodenökologie und Bodengenese: Bodenphysikalische Kennwerte und Berechnungsverfahren für die Praxis. Technische Universität Berlin, Berlin, Germany, p. 51.
Richards, L.A., 1931. Capillary conduction of liquids through porous mediums. Phys. – J. Gen. Appl. Phys. 1 (1), 318–333.
Saxena, R.K., Dressie, Z., 1983. Estimation of groundwater recharge and moisture movement in sandy formations by tracing natural oxygen-18 and injected tritium profiles in the unsaturated zone. In: IAEA (Ed.), Isotope Hydrology in Water Resources Development 1983. Isotope Hydrology, Vienna, pp. 139–150.
Sayama, T., McDonnell, J.J., Dhakal, A., Sullivan, K., 2011. How much water can a watershed store? Hydrol. Process. 25 (25), 3899–3908.
Scherrer, S., 1996. Abflussbildung bei Starkniederschlägen. Identifikation bei Abflussprozessen mittels künstlicher Niederschläge. PhD Thesis, ETH Zürich, Zürich, Switzerland, p. 178.
Schmocker-Fackel, P., 2004. A method to delineate runoff processes in a catchment and its implications for runoff simulations. PhD Thesis, ETH Zürich, Zürich, Switzerland, p. 197.
Schulla, J., Jasper, K., 2007. Model Description WaSiM-ETH. Institute of Geography, ETH Zürich, Zürich, Switzerland.
Seibert, J., McGlynn, B.L., 2007. A new triangular multiple flow direction algorithm for computing upslope areas from gridded digital elevation models. Water Resour. Res. 43 (4).
Shurbaji, A.R.M., Phillips, F.M., 1995. A numerical model for the movement of H2O, H2(18)O, and (2)HHO in the unsaturated zone. J. Hydrol. 171 (1–2), 125–142.
Simunek, J., Jarvis, N.J., van Genuchten, M.T., Gardenas, A., 2003. Review and comparison of models for describing non-equilibrium and preferential flow and transport in the vadose zone. J. Hydrol. 272 (1–4), 14–35.
Soil Survey Division Staff, 1993. Soil survey manual. Soil Conservation Service. U.S. Department of Agriculture, Handbook 18, Washington, USA, p. 315.
Sponagel, H. et al., 2005. Bodenkundliche Kartieranleitung. E. Schweizerbart'sche Verlagsbuchhandlung, Hannover, Germany, p. 438.
Stähli, M., Jansson, P.E., Lundin, L.C., 1996. Preferential water flow in a frozen soil – a two-domain model approach. Hydrol. Process. 10 (10), 1305–1316.
Steelman, C.M., Endres, A.L., 2012. Assessing vertical soil moisture dynamics using multi-frequency GPR common-midpoint soundings. J. Hydrol. 436, 51–66.
Stewart, M.K., McDonnell, J.J., 1991. Modeling base-flow soil–water residence times from deuterium concentrations. Water Resour. Res. 27 (10), 2681–2693.
Stumpp, C., Hendry, M.J., 2012. Spatial and temporal dynamics of water flow and solute transport in a heterogeneous glacial till: the application of high-resolution profiles of delta O-18 and delta H-2 in pore waters. J. Hydrol. 438, 203–214.
Stumpp, C., Maloszewski, P., 2010. Quantification of preferential flow and flow heterogeneities in an unsaturated soil planted with different crops using the environmental isotope δ^{18}O. J. Hydrol. 394 (3–4), 407–415.
Stumpp, C., Stichler, W., Maloszewski, P., 2009. Application of the environmental isotope δ^{18}O to study water flow in unsaturated soils planted with different crops: case study of a weighable lysimeter from the research field in Neuherberg, Germany. J. Hydrol. 368 (1–4), 68–78.
Stumpp, C., Stichler, W., Kandolf, M., Simunek, J., 2012. Effects of land cover and fertilization method on water flow and solute transport in five lysimeters: a long-term study using stable water isotopes. Vadose Zone J. 11 (1), p. vzj2011.0075.
Taylor, S. et al., 2001. Isotopic evolution of a seasonal snowpack and its melt. Water Resour. Res. 37 (3), 759–769.
Uchida, T., Kosugi, K., Mizuyama, T., 2001. Effects of pipeflow on hydrological process and its relation to landslide: a review of pipeflow studies in forested headwater catchments. Hydrol. Process. 15 (11), 2151–2174.
UNESCO-IHE, 2011. Mid-term Research Agenda (2011–2015) of the chair group Hydrology and Water Resources (HWR core).
Van Genuchten, M.T., 1980. A closed form equation for predicting the hydraulic conductivity of unsaturated soils. Soil Sci. Soc. Am. J. 44 (5), 892–898.
van Genuchten, M.T., Simunek, J., 2004. Integrated modeling of vadose zone flow and transport processes. In: Feddes, R.A., de Rooij, G.H., van Dam, J.C. (Eds.), Unsaturated Zone Modelling: Progress, Challenges and Applications. Wageningen UR Frontis Series. Kluwer Academic Publishers, Dordrecht, The Netherlands, pp. 37–69.
van Genuchten, M.T., Wierenga, P.J., 1986. Solute dispersion coefficients and retardation factors. In: Klute, A. (Ed.), Methods of Soil Analysis: Part 1 – Physical and Mineralogical Methods. American Society of Agronomy, Madison, Wisconsin, pp. 1025–1054.
Vanderborght, J., Vereecken, H., 2007. Review of dispersivities for transport modeling in soils. Vadose Zone J. 6 (1), 29–52.
Vereecken, H. et al., 2008. On the value of soil moisture measurements in vadose zone hydrology: a review. Water Resour. Res. 44 (W00D06).
Viviroli, D. et al., 2011. Climate change and mountain water resources: overview and recommendations for research, management and policy. Hydrol. Earth Syst. Sci. 15 (2), 471–504.
Wassenaar, L.I., Hendry, M.J., Chostner, V.L., Lis, G.P., 2008. High resolution pore water delta H-2 and delta O-18 measurements by H2O(liquid)-H2O(vapor) equilibration laser spectroscopy. Environ. Sci. Technol. 42 (24), 9262–9267.
Weiler, M., McDonnell, J.R.J., 2006. Testing nutrient flushing hypotheses at the hillslope scale: a virtual experiment approach. J. Hydrol. 319 (1–4), 339–356.
Weingartner, R., Viviroli, D., Schaedler, B., 2007. Water resources in mountain regions: a methodological approach to assess the water balance in a highland-lowland-system. Hydrol. Process. 21 (5), 578–585.
Wettstein, S., 1999. Grünerlengebüsche in den Schweizer Alpen: Ein Simulationsmodell aufgrund abiotischer Faktoren und Untersuchungen über morphologische und strukturelle Variabilität. Masters Thesis, University of Bern, Bern, Switzerland, p. 62.
Williams, C.J., McNamara, J.P., Chandler, D.G., 2009. Controls on the temporal and spatial variability of soil moisture in a mountainous landscape: the signature of snow and complex terrain. Hydrol. Earth Syst. Sci. 13 (7), 1325–1336.
Zehe, E., Graeff, T., Morgner, M., Bauer, A., Bronstert, A., 2010. Plot and field scale soil moisture dynamics and subsurface wetness control on runoff generation in a headwater in the Ore Mountains. Hydrol. Earth Syst. Sci. 14 (6), 873–889.